Ultrasound in Med. & Biol., Vol. 42, No. 1, pp. 308–321, 2016

0301-5629/$ - see front matter

http://dx.doi.org/10.1016/j.ultrasmedbio.2015.08.012

● *Original Contribution*

ARTERIAL STIFFNESS ESTIMATION BY SHEAR WAVE ELASTOGRAPHY: VALIDATION IN PHANTOMS WITH MECHANICAL TESTING

Elira Maksuti,*† Erik Widman,*† David Larsson,* Matthew W. Urban,‡ Matilda Larsson,*† and Anna Bjällmark*†

*Department of Medical Engineering, School of Technology and Health, KTH Royal Institute of Technology, Stockholm, Sweden; †Department of Molecular Medicine and Surgery, Karolinska Institutet, Solna, Sweden; and ‡Department of Physiology and Biomedical Engineering, Mayo Clinic College of Medicine, Rochester, Minnesota, USA

(*Received* 13 *March* 2015; *revised* 7 *July* 2015; *in final form* 17 *August* 2015)

Abstract—Arterial stiffness is an independent risk factor found to correlate with a wide range of cardiovascular diseases. It has been suggested that shear wave elastography (SWE) can be used to quantitatively measure local arterial shear modulus, but an accuracy assessment of the technique for arterial applications has not yet been performed. In this study, the influence of confined geometry on shear modulus estimation, by both group and phase velocity analysis, was assessed, and the accuracy of SWE in comparison with mechanical testing was measured in nine pressurized arterial phantoms. The results indicated that group velocity with an infinite medium assumption estimated shear modulus values incorrectly in comparison with mechanical testing in arterial phantoms (6.7 ± 0.0 kPa from group velocity and 30.5 ± 0.4 kPa from mechanical testing). To the contrary, SWE measurements based on phase velocity analysis (30.6 ± 3.2 kPa) were in good agreement with mechanical testing, with a relative error between the two techniques of 8.8 ± 6.0% in the shear modulus range evaluated (40–100 kPa). SWE by phase velocity analysis was validated to accurately measure stiffness in arterial phantoms. (E-mail: elira.maksuti@sth.kth.se) **© 2016 The Authors. Published by Elsevier Inc. This is an open access article under the CC BY-NC-ND license (http://creativecommons.org/licenses/by-nc-nd/4.0/).**

Key Words: **Accuracy, Arterial phantom, Arterial stiffness, Group velocity, Lamb waves, Mechanical testing, Phase velocity, Poly(vinyl alcohol), Shear modulus, Shear wave elastography.**

INTRODUCTION

Arterial stiffness has been reported to be an independent risk factor for a wide range of cardiovascular diseases, such as hypertension, heart failure, stroke (Quinn et al. 2012; Vlachopoulos et al. 2010) and hypertensive complications of pregnancy (Coutinho 2014). Furthermore, elevated arterial stiffness is a marker for the development of atherosclerosis (Vlachopoulos et al. 2010) that may precede the onset of clinical apparent cardiovascular disease as well as be involved in the development of hypertension (Glasser 1997). Early detection of elevated arterial stiffness therefore has the potential to improve diagnosis and decrease morbidity and mortality rates.

Several methods have been suggested to estimate *in vivo* arterial stiffness globally and locally. The pulse wave velocity (PWV) technique is commonly used to estimate global arterial stiffness by measuring the velocity of the pulse wave generated by the heart while propagating through the arterial system. This PWV is then related to the arterial elastic modulus of the arterial wall. Other methods aim at estimating indices related to local arterial stiffness and are usually based on ultrasound imaging techniques. Among these methods, some common measures are distensibility (Hoeks et al. 1990), stiffness index (Kawasaki et al. 1987), local PWV imaging (Brands et al. 1998), arterial wall strain (Ribbers et al. 2007) and arterial wall strain–stress elastography (Khamdaeng et al. 2012). However, these are often combined with pressure measurements that are performed in peripheral arteries by tonometry and apply a transfer function to obtain the pressure waveform in the large central arteries (Kim and Braam 2013). Because of the limitations of the suggested methods, no gold standard for assessing arterial stiffness locally has been identified (Hamilton et al. 2007).

In the past few decades, there has been increased interest in the ultrasound technique shear wave

Address correspondence to: Elira Maksuti, School of Technology and Health, KTH Royal Institute of Technology, Alfred Nobels Allé 10, 141 52 Huddinge, Sweden. E-mail: elira.maksuti@sth.kth.se

elastography (SWE) (Sarvazyan et al. 2013). SWE is a non-invasive tool used to quantitatively assess local tissue stiffness that can be integrated into a conventional ultrasound device (Bercoff et al. 2004a). The technique takes advantage of the fact that the speed of shear waves is related to the elastic shear modulus of the material. SWE has so far been validated and clinically adapted for large and relatively homogeneous organs such as breast (Chang et al. 2011) and liver (Ferraioli et al. 2014). In these organs, the shear waves are assumed to travel in a purely elastic infinite medium. In such case, the linear elastic shear modulus μ can be derived from the density ρ of the tissue and the shear wave speed c_s by

$$\mu = \rho c_s^2 \tag{1}$$

Commercial SWE systems are based on these assumptions and, therefore, specifically developed for large organs. In these systems, the speed of the envelope of the propagating shear wave, also referred to as group velocity, is used to calculate the shear modulus. The assumption of a large, homogeneous, infinite, elastic medium does not hold for arteries, but, despite this, commercially available ultrasound SWE systems have been used in arterial applications both *in vitro* (Ramnarine et al. 2014) and *in vivo* (Garrard and Ramnarine 2014). Initial studies for clinical applications of ultrasound SWE in confined tissues, such as the arterial wall (Bernal et al. 2011; Couade et al. 2010), bladder (Nenadic et al. 2013) and cornea (Tanter et al. 2009), have recently been carried out.

Magnetic resonance elastography methods have also been developed to derive arterial stiffness from the speed of induced shear waves (Woodrum et al. 2006; Xu et al. 2012). Magnetic resonance elastography enables imaging of central arteries such as the aorta, which can be difficult to image with ultrasound, but has the disadvantage of lower spatial and temporal resolution compared with ultrasound. Also the arterial magnetic resonance studies have based their analysis on group velocity.

In a confined geometry, shear wave propagation is strongly affected by internal reflections at the medium's boundaries, resulting in guided wave propagation. These reflections generate dispersion (*i.e.*, waves at different frequencies travel at different speeds), such as seen in viscoelastic media, even if the medium itself is purely elastic (Chen et al. 2004). This guided wave propagation can be mathematically modeled. An analytical solution for wave propagation in a hollow cylinder, with geometry close to that of an artery, has previously been derived (Gazis 1959a). However, the solution includes a series of Bessel functions, which can only be determined numerically (Gazis 1959b). To reduce the complexity, while still taking the geometric dispersion phenomenon into account, adoption of a Lamb wave propagation model in a plate and approximation of the complex propagation in the artery with a zero-order anti-symmetric Lamb wave mode has been proposed (Bernal et al. 2011; Couade et al. 2010). This simplification can be justified by the fact that the dispersion curves (*i.e.*, phase velocity–frequency relationship) of the plate and the hollow cylinder converge at higher frequencies (Couade et al. 2010). The expression for the anti-symmetric Lamb wave mode for a solid plate submerged in a non-viscous incompressible fluid, assuming that the solid plate and surrounding fluid have similar densities and wavenumbers, is given by (Bernal et al. 2011)

$$4k_L^3\beta \cosh\left(k_L\frac{h}{2}\right)\sinh\left(\beta\frac{h}{2}\right) - \left(k_s^2-2k_L^2\right)^2 \sinh\left(k_L\frac{h}{2}\right)\cosh\left(\beta\frac{h}{2}\right) = k_s^4 \cosh\left(k_L\frac{h}{2}\right)\cosh\left(\beta\frac{h}{2}\right) \tag{2}$$

where $k_L = \omega/c_L$ is the Lamb wavenumber, $k_S = \omega\sqrt{\rho/\mu}$ is the shear wavenumber, $\beta = \sqrt{k_L^2-k_s^2}$, ω is the angular frequency, h is the plate thickness and c_L is the frequency-dependent Lamb wave velocity. Because k_s and β are functions of the elastic shear modulus, the latter can be derived by fitting the experimental data to the theoretical model.

Phase velocity analysis using eqn (2) has previously been applied to assess arterial stiffness in urethane tubes and excised porcine carotid arteries using a Lamb wave-based model (Bernal et al. 2011), as well as in arterial phantoms and *in vivo*, where an empirical formula derived from Lamb wave theory was used to estimate the shear modulus (Couade et al. 2010). However, comparison with an independent reference method was not reported in these studies. In addition, a study of the feasibility of using SWE for detection of arterial nonlinear behavior and anisotropy on a single equine aortic sample, with comparison with mechanical testing, was recently published (Shcherbakova et al. 2014). In this study, only group velocity analysis was performed, and the sample was cut longitudinally before ultrasound investigation, thereby losing its cylindrical geometry.

Even though efforts have been made to improve the ability to apply SWE in arterial applications, the accuracy of SWE measurements in a hollow cylindrical geometry compared with a reference method has not been evaluated yet. Therefore, this study aimed at experimentally investigating the influence of a confined geometry in shear modulus estimation with SWE in order to determine if group velocity could be used to derive an acceptable approximation of shear modulus for arterial applications or if phase velocity analysis is needed. Another aim was to assess the accuracy of the optimal SWE analysis method for arterial applications *in vitro*.

METHODS

This study was divided into two parts: a geometry study and an accuracy study. The aim of the geometry study was to investigate the influence of confined geometry on SWE shear modulus estimation by constructing phantoms with three different geometries (plate, solid cylinder and hollow cylinder). In the initial geometry study, SWE based on both group velocity and phase velocity analysis was compared with mechanical testing to determine the most accurate analysis for arterial applications. In the accuracy study, the aim was to assess the accuracy of SWE for arterial applications by comparing the SWE results from nine phantoms mimicking the common carotid artery with reference values obtained from mechanical testing at different intraluminal pressures, using the analysis that performed best in the geometry study.

Phantom construction

The phantoms were made of poly(vinyl alcohol) (PVA) cryogel, proven to be a suitable tissue-mimicking material for ultrasound elastography methods (Fromageau et al. 2007). With PVA, stiffness can be controlled and varied by adjusting the number of freeze/thaw (F/T) cycles during manufacturing, where larger numbers of cycles correspond to stiffer material. A solution in mass percentage of 87% de-ionized water, 10% fully hydrolyzed PVA (molecular weight: 56.140 g/mol, density: 1.269 g/cm^3, Sigma-Aldrich, St. Louis, MO, USA) and 3% graphite powder (molecular weight: 12.01 g/mol, density: 5 g/cm^3, particle size <50 μm, Merck KGaA, Darmstadt, Germany) was heated to approximately 65°C, while continuously being stirred, and successively poured into phantom molds of various geometric shapes.

For the geometry study, six phantoms of different shapes were constructed, two for each shape represented in Figure 1. The PVA solution was poured into phantom molds with the shape of a plate (a), a solid cylinder (b) and a hollow cylinder (c). For more details on the hollow cylinder construction, that is, the arterial phantom (shape c), the reader is referred to a previous study (Larsson et al. 2015). The six phantoms underwent three F/T cycles (12 h at a room temperature of approximately 22°C, 12 h at −23°C) and were manufactured at the same time and from the same batch of PVA.

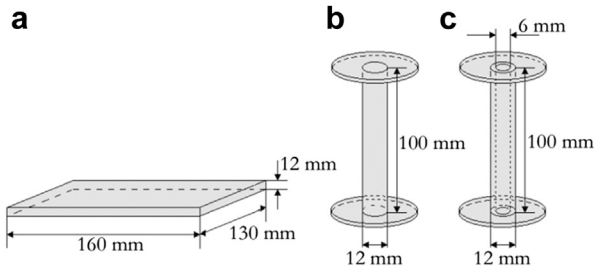

Fig. 1. Differently shaped poly(vinyl alcohol) cryogel phantoms used to determine the influence of geometry on shear wave propagation and shear modulus estimation in the geometry study: (a) plate; (b) solid cylinder; (c) hollow cylinder.

For the accuracy study, nine common carotid artery phantoms were constructed with shapes and dimensions as in Figure 1c. To obtain phantoms with different stiffness values, the arterial phantoms were exposed to three, four and five F/T cycles, respectively (three phantoms for each condition). The number of phantoms for each shape constructed for the geometry and accuracy studies is given in Table 1.

Shear wave elastography

Shear wave elastography data were retrieved from all PVA phantoms submerged in water, with some experimental differences between the geometry and accuracy studies as described in the following sections.

Experimental setup

Geometry study. During SWE investigations, the plate (Fig. 1a) was placed in a polypropylene container and submerged in water at approximately 15°C–20°C. The solid cylinder and hollow cylinder (Fig. 1b, c) were connected to a customized enclosure, as illustrated in Figure 2.

Accuracy study. To better reproduce an *in vivo* stress state, the arterial phantoms were pressurized. The constructed enclosure (Fig. 2a) allowed for pressurization

Table 1. Number of phantoms constructed for each geometry

	Plate	Solid cylinder	Hollow cylinder
Geometry study	2	2	2
Accuracy study	—	—	9

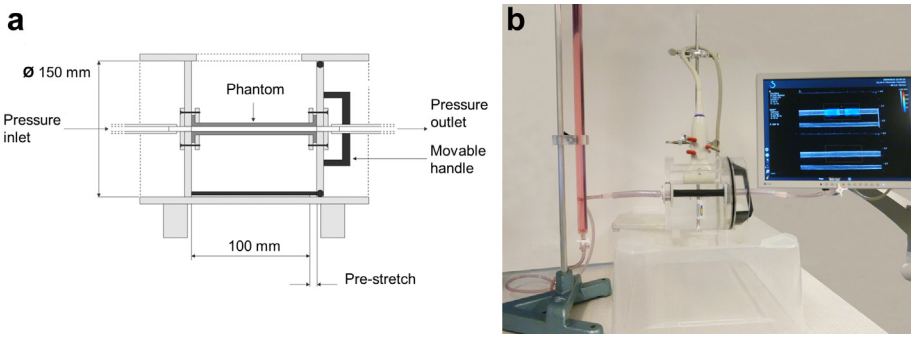

Fig. 2. (a) Cross-sectional schematic of a poly(vinyl alcohol) arterial phantom mounted in the customized enclosure used during shear wave elastography measurements. (b) Photograph of the shear wave elastography acquisition setup, in which an arterial phantom is mounted in the customized enclosure, connected to the water column and imaged with the ultrasound system.

of the arterial phantom lumen through the pressure inlet and outlet. The pressure inlet was connected to a water column generating four different intraluminal pressures of 60, 80, 100 and 120 mm Hg, respectively, with the pressure outlet being closed. An example of a PVA arterial phantom, mounted to the enclosure, connected to the water column and submerged in water is illustrated in Figure 2b. The water in the column was colored to more easily identify the water level and possible leakage. Once pressurized, the phantoms experienced a longitudinal elongation, which was compensated by a controlled pre-stretch to avoid phantom bulging. This elongation was estimated by calculating the stress σ_z imposed by an intraluminal pressure p in a thin-walled hollow cylinder in the direction of the cylinder's long axis, which is given by the eqn

$$\sigma_z = \frac{pR}{2h} \tag{3}$$

with R and h being the average radius and thickness of the arterial phantom given by the mold dimensions. The reaction force on the same axis F_z was then calculated as

$$F_z = \frac{pRA}{2h} \tag{4}$$

with A being the cross-sectional area of the arterial phantom as per construction. The pressurized phantoms were connected to a mechanical tensile testing machine (Instron 5567, Instron, Norwood, MA, USA). The distance between the plates of the testing machine was gradually increased until the load cell, calibrated to 0 N at the phantom's initial length of 10 cm, reported the reaction force F_z previously calculated. At this point, the pre-stretch was measured as the difference between the final and initial phantom lengths. Calculated reaction forces and resulting pre-stretches for different static pressures are reported in Table 2. The resulting pre-stretch was recorded for each phantom and used for both mechanical testing and SWE measurements to guarantee the same loading conditions for the two methods. In the SWE measurements, the pre-stretch was applied to the long axis of the phantom by a movable end fixation at the right extremity of the enclosure, as schematically illustrated in Figure 2a.

Data acquisition

The ultrasound data were acquired with the commercially available Aixplorer system (SuperSonic Imagine, Aix-en-Provence, France) with a SuperLinear SL15-4 transducer. The ultrasound machine was modified with a customized research package, allowing for export of the in-phase and quadrature (IQ) data. Acoustic radiation force excitation (also referred to as "push") and ultrafast image acquisition were carried out using the same system. The Aixplorer system generates shear waves by means of the technique called supersonic shear imaging (SSI), where consecutive multiple pushes of 150 μs each are located at different depths along a defined line. Because of the induction of multiple pushes, the wavefront of the generated shear wave has higher amplitude (Bercoff et al. 2004b) and therefore is easier to detect.

Table 2. Calculated long-axis reaction force and resulting pre-stretch used in the accuracy study*

Applied intraluminal pressure (mm Hg)	Long-axis reaction force (N)	Pre-stretch (mm)		
		3 F/T cycles	4 F/T cycles	5 F/T cycles
60	0.509	7.4 ± 1.2	4.6 ± 0.6	4.7 ± 0.9
80	0.679	9.6 ± 1.5	6.0 ± 0.8	6.2 ± 1.2
100	0.848	12.7 ± 3.4	7.3 ± 1.0	7.6 ± 1.5
120	1.018	13.7 ± 1.8	8.5 ± 1.1	8.8 ± 1.7

F/T = freeze/thaw.
* Means ± SD were calculated from three phantoms for each F/T cycle and intraluminal pressure level.

These consecutive single pushes are also referred to as a supersonic push (Bercoff et al. 2004a).

In the geometry study, the transducer was placed approximately 10 mm above the phantom surface. A region of interest (ROI), with height and width of approximately 10 and 20 mm was positioned such that the second push location of the supersonic push (comprising a total of three single pushes 5 mm from each other) was placed in the middle of the phantom. For the hollow cylinder, the ROI was placed first in the middle of the anterior wall and then in the middle of the posterior wall, corresponding to the upper and lower phantom wall in the ultrasound image. Three repeated acquisitions were performed for each ROI location, with an interval of 100 ms between consecutive acquisitions. The operating frequency of the transducer was 5 MHz in pushing mode and 7.5 MHz in ultrafast imaging mode. The pulse repetition frequency was set to 8000 Hz, and 42 frames were acquired after each supersonic push generation.

In the accuracy study, all data were acquired as in the geometry study for the hollow cylinder.

Post-processing

The IQ data exported from the ultrasound machine were processed using MATLAB R2013b. First, five adjacent tracking lines parallel to the surface of the transducer were manually selected in the middle of the phantom wall. Second, axial displacement over time along each line was estimated using a 2-D autocorrelation algorithm (Loupas et al. 1995), which was found to perform as well as the gold standard normalized cross-correlation, but with a significantly faster computation time (Pinton et al. 2006). The axial displacement estimation $\overline{u}$ derived from the IQ data can be written as

$$\overline{u} = \frac{c}{4\pi f_c} \frac{\arctan\left(\frac{\sum_{m=0}^{M-1}\sum_{n=0}^{N-2}[Q(m,n)I(m,n+1)-I(m,n)Q(m,n+1)]}{\sum_{m=0}^{M-1}\sum_{n=0}^{N-2}[I(m,n)I(m,n+1)+Q(m,n)Q(m,n+1)]}\right)}{1+\arctan\left(\frac{\sum_{m=0}^{M-2}\sum_{n=0}^{N-1}[Q(m,n)I(m+1,n)-I(m,n)Q(m+1,n)]}{\sum_{m=0}^{M-2}\sum_{n=0}^{N-1}[I(m,n)I(m+1,n)+Q(m,n)Q(m+1,n)]}\right)\Big/2\pi} \quad (5)$$

with c being the speed of sound for compressional waves, f_c the center frequency of the radio frequency (RF) signal and I and Q the in-phase and quadrature components of the RF signal.

The axial displacement was then averaged over the selected tracking lines, generating the axial displacement map in Figure 3. For the geometry study, the shear modulus was calculated using group velocity with an infinite medium assumption (group velocity analysis), as well as the phase velocity and plate model approach (phase velocity analysis). The steps of the phase velocity analysis are summarized in Figure 3.

Group velocity c_g was estimated by computing the Radon transform of the axial displacement map, representing the sum of all the pixel values over straight lines in the image, oriented at different angles (Song et al. 2013). The maximum of the Radon transform was then selected to retrieve the angle of the most significant wavefront of the propagating shear wave. This angle is directly related to the speed of the shear wave. Given c_g and assuming an infinite homogeneous medium, the shear modulus was derived as per eqn (1), with $c_s = c_g$.

The phase velocity c_p as a function of frequency (dispersion curve) was obtained using Fourier analysis. A 2-D discrete fast Fourier transform of the axial displacement map was performed to transform the space–time domain into the wavenumber–frequency domain (also denoted as k-space) (Bernal et al. 2011). An amplitude mask, which removed signals with amplitude $<10\%$ of the maximum intensity of the entire k-space, was applied to reduce background noise. Subsequently, the k-space was converted into a phase velocity–frequency space by relating the wave number (k_L) to the phase velocity (c_p) through

$$c_p = \frac{f}{k_L} \quad (6)$$

with f being the frequency at each specific position in the phase velocity–frequency map. This is referred to as the phase velocity–intensity map in Figure 3. The dispersion curve was then obtained by selecting the phase velocity at which the intensity was maximal for each frequency. To improve the robustness of the dispersion curve estimation, two cutoff limits were introduced: a lower cutoff defined by the frequency for which the relative change between neighboring values was $>50\%$ (removing high-intensity signal around 0 Hz), and a higher cutoff defined by the frequency for which the intensity had decreased to $<30\%$ of the maximum intensity (removing the part of the signal with low signal-to-noise ratio). The final

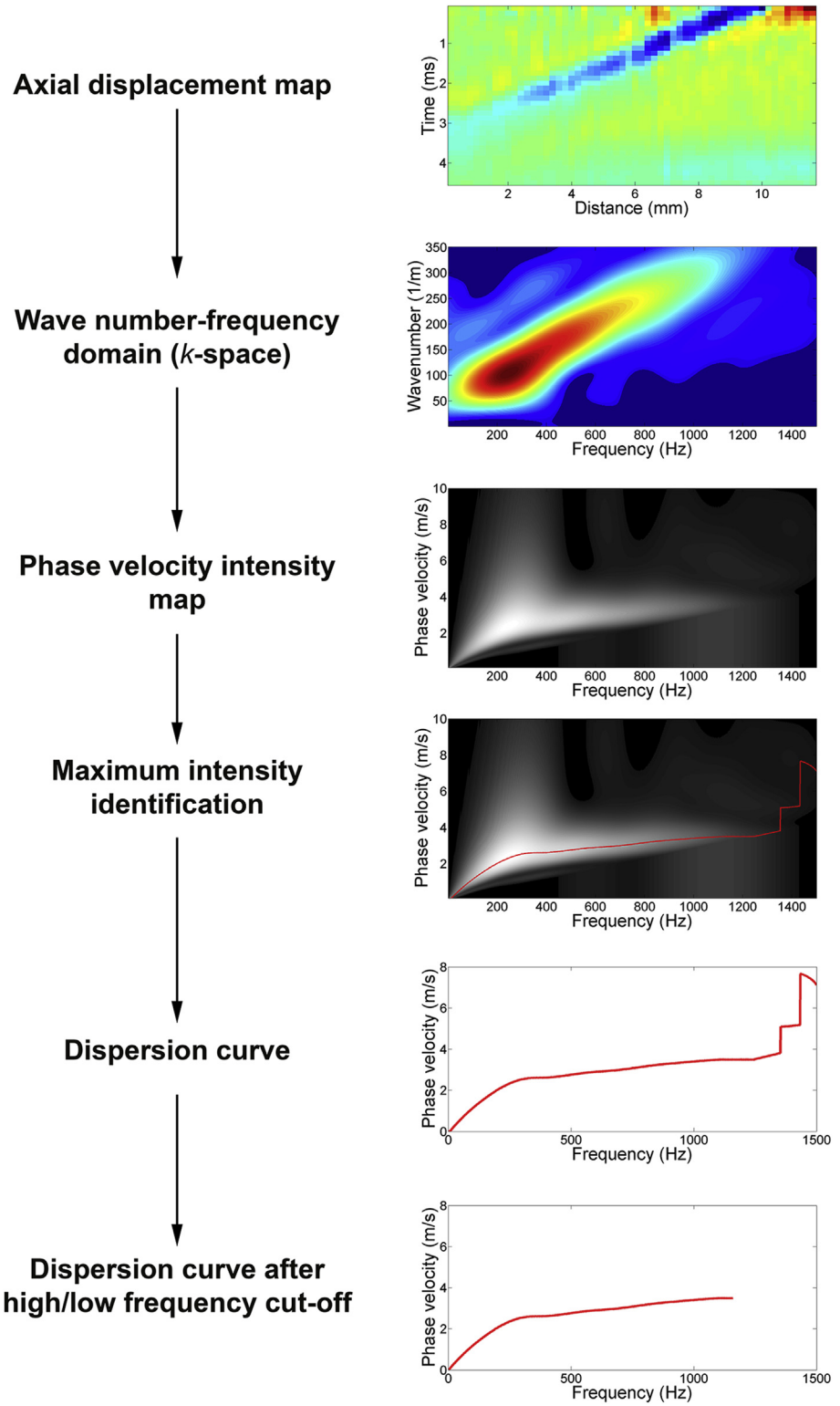

Fig. 3. Schematic description of the main steps of the shear wave elastography post-processing used to derive phase velocity as a function of frequency (dispersion curve).

dispersion curve was then fit by linear least squares to eqn (2) where $c_p = c_L$. Plate thickness h, corresponding to the phantom wall thickness, varied with different pressure levels for the arterial phantoms and was measured in the ultrasound image using the distance function of the Aixplorer system before being introduced as an input to

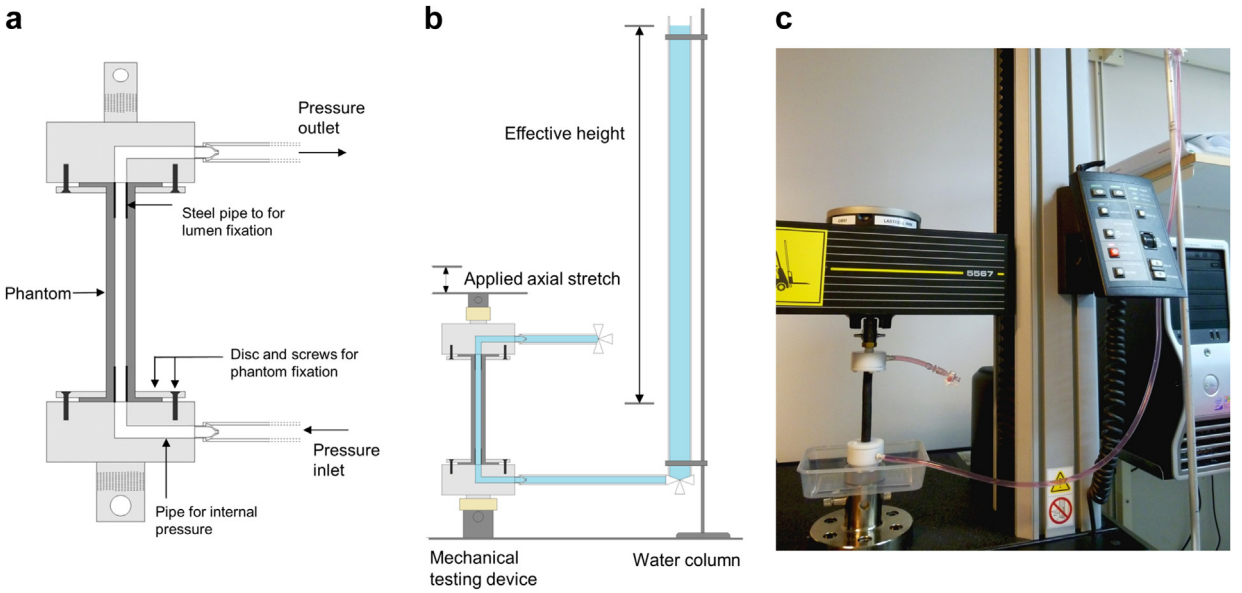

Fig. 4. (a) Schematic representations of the mechanical test setup for the arterial phantom with customized end fixtures and (b) connection to the water column for pressurization. Note that for illustrative purposes, the proportions of the phantom and the water column in (b) do not represent real proportions. (c) Photograph of the arterial phantom connected to the mechanical testing device and to the water column during experiments.

eqn (2). The shear modulus was therefore the only parameter that varied during the iterative curve-fitting procedure. The curve fitting was computed for the entire signal spectrum, as well as for frequencies >500 Hz and up to the high cutoff limit. This was done because the phase velocities differ from those of the plate model mainly at low frequencies, where the dispersion curve of the hollow cylinder shows a characteristic local decrease (Couade et al. 2010). After evaluation of the results from the geometry study, only phase velocity analyses for frequencies >500 Hz were considered in the accuracy study.

Mechanical testing

For the geometry study, the shear modulus estimated by SWE for all three geometries was compared with the shear modulus of an additional reference cylindrical sample phantom (height and diameter of 40 mm). The sample phantom was manufactured at the same time and with the same material as the other three geometries and tested under the same stress configuration as the other geometries (neither pressurization nor prestretch). The mechanical testing on the sample cylinder was performed by imposing 10% strain in uniaxial compression using an MTS Insight 100-kN mechanical testing system (MTS Systems, Eden Prairie, MN, USA) combined with a 10-kg load cell of ±100-N capacity and a calibrated maximum displacement error equal to 0.03%.

For the accuracy study, the PVA phantoms were mounted on the mechanical testing device Instron 5567 by means of customized end fixtures, prestretched and pressurized, to mimic the same loading conditions as for the SWE measurements. The prestretch was applied by moving the upper fixation of the testing device to a higher starting position to ensure the same stress state between the mechanical testing and SWE setup, accounting for potential non-linear behavior of the PVA. Figure 4 is a schematic of the mechanical testing setup for the accuracy study. The test for the pressurized arterial phantoms was performed by applying deformation-controlled axial tension starting from 0 to 10% strain at the rate of 10 mm/min. Successively, data recorded from the machine (axial force F_z and axial deformation δ_z) were used to calculate the principal stretch λ_z and the axial stress σ_z, defined as

$$\lambda_z = \frac{\delta_z + L_\mathrm{i}}{L_\mathrm{i}} \tag{7}$$

$$\sigma_z = \frac{F_z \lambda_z}{A_i} \tag{8}$$

with L_i denoting the initial length and A_i the initial cross-sectional area of the sample. Because the PVA samples exhibited approximately linear behavior in the experimental deformation range, linear theory was used. The linear relation between axial stress σ_z and strain ε_z for an incompressible material based on Hooke's law is

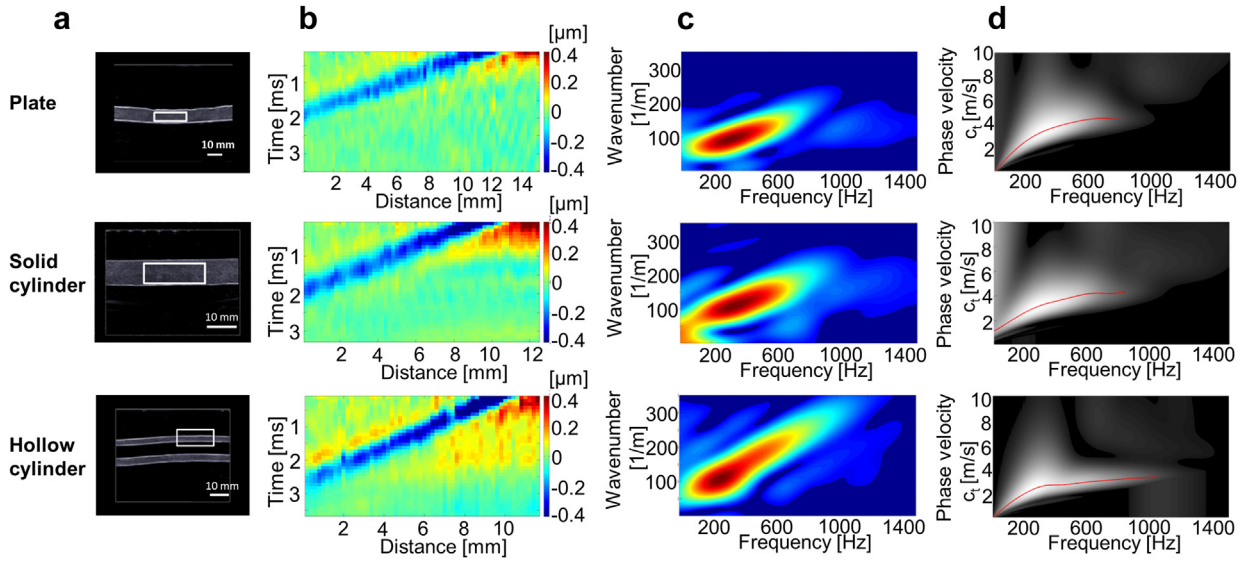

Fig. 5. Shear wave propagation and phase velocity analysis for the three phantom geometries. (a) Ultrasound image of the phantom with the region of interest selected for the shear wave elastography measurement. (b) Axial displacement map. (c) *k*-Space and (d) phase velocity intensity maps.

$$\sigma_z = E\varepsilon_z \tag{9}$$

$$\varepsilon_Z = \lambda_z - 1 \tag{10}$$

where E is the material's linear elastic Young's modulus. For each arterial phantom, a mean value for E was estimated using piecewise linearization, where the stress–strain curve was first divided into sub-segments of 30 measurement points each. Second, least-squares fit linearization was applied and E obtained for each sub-segment. Successively, the E values derived from each sub-segment were averaged together to obtain a

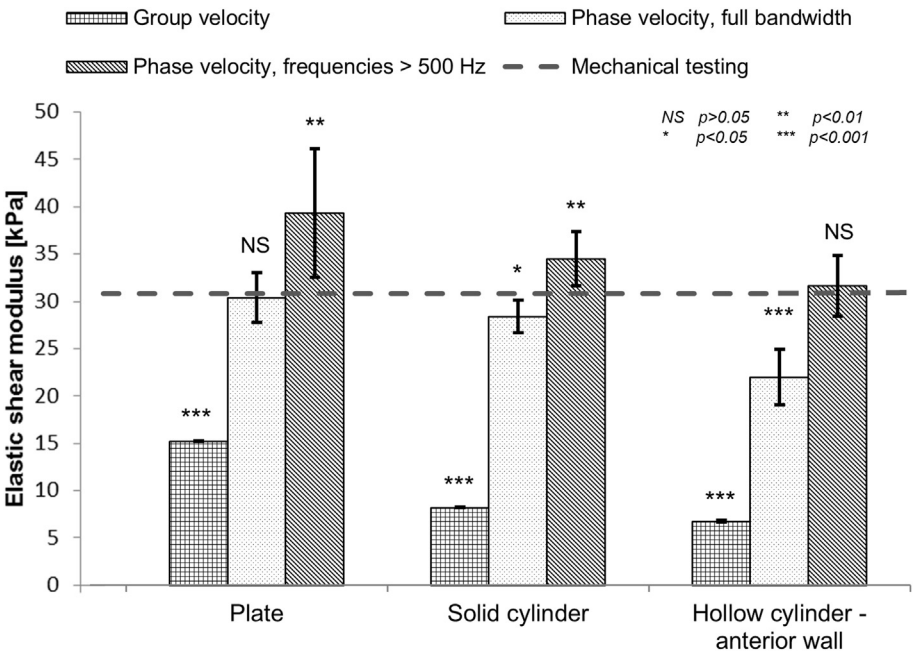

Fig. 6. Comparison of shear moduli obtained using mechanical testing and shear moduli obtained using different post-processing procedures for the phantoms in the geometry study. The *p*-value indicates the statistical significance between the different analysis methods and mechanical testing.

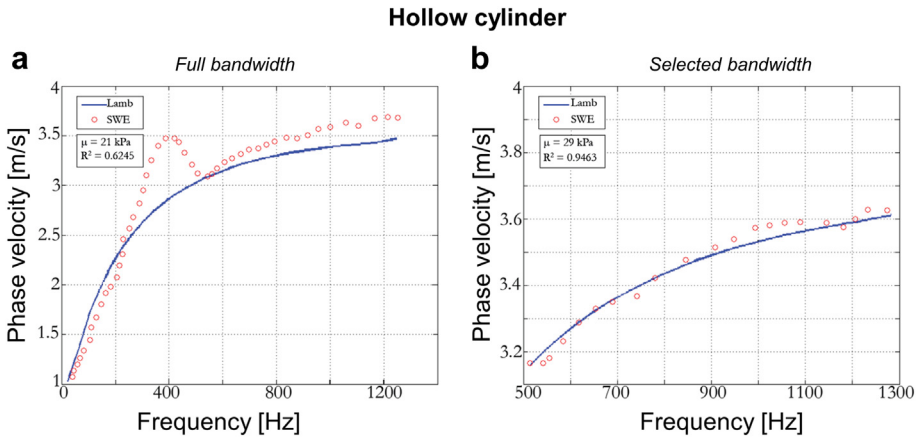

Fig. 7. Sample experimental dispersion curve for the hollow cylinder (arterial phantom). (a) Dispersion curve measured with SWE (*red dots*) and the best theoretical fit for a plate submerged in a non-viscous liquid (*blue line*), for the full bandwidth. (b) Experimental SWE dispersion curve and best theoretical fit for frequencies >500 Hz. SWE = shear wave elastography.

mean Young's modulus [29]. Finally, given the isotropy and incompressibility of the phantom material (Fromageau et al. 2003), the shear modulus μ was derived using

$$E = 3\mu \tag{11}$$

For both the geometry and accuracy studies, the PVA phantoms were stored in water at room temperature, mounted and tested within a short time to avoid potential effects of dehydration.

Statistical analysis

For the geometry study, the difference between the shear modulus estimated with the different SWE analysis methods (group velocity, phase velocity full bandwidth and phase velocity >500 Hz) and the shear modulus estimated by mechanical testing was tested against a zero mean distribution using a one-sample *t*-test. For the accuracy study, the difference in SWE-measured shear moduli between the anterior and posterior arterial phantom walls (for each phantom and condition) was also tested against a zero mean distribution using a one-sample *t*-test. The distributions of the relative errors between SWE measurements and mechanical testing, grouped for different values of intraluminal pressure, number of F/T cycles and ROI placement, were tested using a paired-sample *t*-test. Statistical analysis was performed using MATLAB R2013b. All data were expressed as means ± SD, and a p value < 0.05 was considered to indicate significance.

RESULTS

Geometry study

Visual assessment of the shear wave propagation maps in the PVA phantoms with different geometries (Fig. 5) revealed experimentally how geometry can influence shear wave propagation through the medium. Figure 5 illustrates shear wave propagation in the time (b) and frequency (c, d) domains for the three different phantom geometries. The axial displacement map (Fig. 5b) featured a noisier and broader front wave for the hollow cylinder (*i.e.*, arterial phantom) compared with the other geometries. All phantoms exhibited some dispersion in the *k*-space because of the combined effect of PVA viscoelasticity (Yang 2008) and confined geometry. For the plate and solid cylinder, the dispersion curve (Fig. 5d, in *red*) was similar to a theoretical dispersion curve for a plate. For the hollow cylinder, the dispersion curve (Figs. 5d and 7a) was similar to that for a hollow cylinder with a characteristic local decrease in phase velocity immediately after 400 Hz. The intensity of the signal at higher frequencies, up to approximately 1 kHz, and the total bandwidth were greater for the thin hollow cylinder than for the other geometries.

Results from the geometry study indicated that the group velocity with an infinite medium assumption incorrectly estimated shear wave values in the hollow cylinder in comparison with mechanical testing (Fig. 6). The mean shear moduli estimated with SWE and the corresponding reference values obtained via mechanical testing for the geometry study are illustrated in Figure 6. For the plate phantoms, the best estimation was provided by the phase velocity approach including the full bandwidth, and was not statistically significantly different from the results of mechanical testing. Phase velocity provided a better estimation also for the solid cylinder when compared with group velocity, although shear modulus was underestimated when considering the full bandwidth and overestimated when considering only high frequencies. The phase velocity analysis with a lower cutoff at 500 Hz

resulted in the best estimation for the hollow cylinder, which was not statistically significantly different from the results of mechanical testing. The shear modulus estimation for the remaining two types of SWE analysis in the hollow cylinder (group velocity and phase velocity full bandwidth) was significantly different from that of mechanical testing, with phase velocity analysis full bandwidth resulting in a smaller error than group velocity.

The difference between shear moduli obtained when considering phase velocity for the full bandwidth and for frequencies >500 Hz is illustrated in Figure 7, which provides the experimental data for phase velocity in the hollow cylinder phantom (*red circles*) and the theoretical plate model phase velocity (*blue line*). The curve fit was performed for all frequencies in Figure 7a and only for frequencies >500 Hz in Figure 7b. The experimental dispersion curve in the hollow cylinder differed from that in the plate model mainly at low frequencies, where it exhibited the characteristic local decrease of a hollow cylinder dispersion curve (Bernal et al. 2011; Couade et al. 2010). After approximately 500 Hz, the two dispersion curves converged, suggesting that only high frequencies of the plate model should be used for the accuracy study.

Accuracy study

Mean shear moduli measured with SWE and mechanical testing for the arterial phantoms at different static pressures and F/T cycles are illustrated in Figure 8. Mean shear modulus values and corresponding standard deviations are also reported in Table 3. As expected, stiffness increased with the number of F/T cycles and with increasing intraluminal pressure, for most phantoms. There was good agreement between SWE and mechanical testing, with a mean absolute error of 5.6 ± 4.1 kPa, corresponding to a relative error of 8.8 ± 6.0%. The relative error did not significantly vary between measurements when grouped for different values of intraluminal pressure, F/T cycles and ROI placement (Table 4). This implies that phase velocity analysis is applicable when performing SWE for assessment of arterial stiffness. There were no statistically significant differences in SWE-measured shear moduli between the anterior and posterior walls of the arterial phantoms.

DISCUSSION

The aim of the present study was to determine the influence of confined geometry in shear modulus estimation via SWE and to measure the accuracy of SWE for assessment of arterial stiffness *in vitro*. Results indicate a good agreement between SWE via phase velocity analysis >500 Hz and mechanical testing in arterial phantoms (Fig. 8), with an average relative error of 8.8 ± 6.0% between SWE and mechanical testing, independent of applied intraluminal pressure, phantom stiffness or ROI location (Table 4).

The results indicate that it is possible to approximate the complex propagation in the arterial phantom with the zero-order anti-symmetric Lamb wave model in a plate submerged in an incompressible, non-viscous fluid with an absolute accuracy of 5.6 ± 4.1 kPa in the shear modulus range evaluated (40–100 kPa). Although previous studies have used phase velocity analysis to estimate arterial stiffness (Bernal et al. 2011; Couade et al. 2010), a validation study of the phase velocity analysis was lacking in the literature. To our knowledge, this is the first accuracy assessment study of SWE in a hollow cylindrical geometry by comparison with mechanical testing. A repeatability study of SWE in arterial phantoms was previously published using the same commercial device as in this study, but based on an infinite medium assumption and group velocity analysis (Ramnarine et al. 2014). Even the vascular magnetic resonance-based studies did not take guided wave propagation into account (Woodrum et al. 2006; Xu et al. 2012). Results in Figure 6 clearly illustrate that the infinite medium assumption, in combination with group velocity analysis, does not correctly estimate shear modulus values in comparison with mechanical testing when shear waves propagate in a thin medium. In this case, geometric dispersion phenomena must be taken into account. SSI was recently applied *ex vivo* on a single sample of equine aortic tissue under dynamic uniaxial loading and different ultrasound probe orientations to study arterial anisotropy (Shcherbakova et al. 2014). This was a feasibility study in which the aortic tissue was cut at two locations and opened longitudinally, thereby losing its cylindrical shape. Phase velocity analysis was not considered because dispersion was not visually detectable in the acquired data, and SWE measurements reported Young's modulus values significantly higher than those of mechanical testing. Nevertheless, the study illustrated the feasibility of using SWE to detect differences in fiber orientation, but highlighted at the same time the need to use more adequate post-processing for accurate shear modulus estimation.

Geometry study

Phantoms with different geometries were manufactured to determine the best analysis method to estimate the shear modulus from shear wave propagation data. The plate geometry was chosen because it corresponds to the Lamb wave model adopted in the phase velocity analysis. The solid cylinder represents an intermediate step between the plate and the geometry of interest in arterial applications, that is, the hollow cylinder or arterial phantom. Results from the geometry study can be

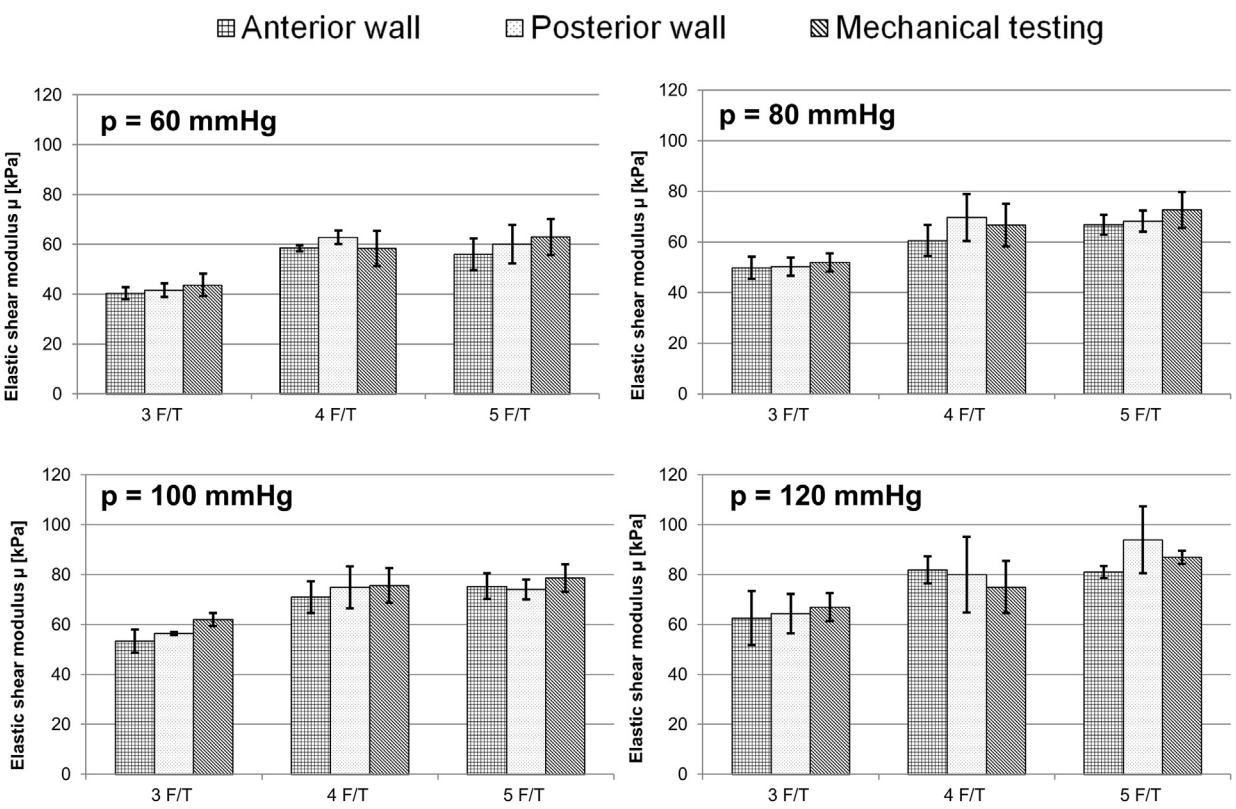

Fig. 8. Comparison of shear moduli for the anterior and posterior walls of the arterial phantoms for different freeze/thaw cycles at different values of intraluminal pressure measured with shear wave elastography and with mechanical testing. Error bars represent the standard deviations of the estimated shear modulus over the three repeated measurements for each phantom and among all phantoms with the same number of freeze/thaw cycles. The difference between the anterior and posterior wall shear wave elastography measurements was not statistically significant.

of relevance also for other shear wave applications in thin tissues such as bladder and cornea, where phase velocity analysis has already been applied (Nenadic et al. 2013; Tanter et al. 2009).

Accuracy study

Although the arterial phantoms used in the accuracy study had a thicker wall (h = 3 mm) than the human common carotid artery (approximately 1 mm), dispersion

Table 3. Comparison of shear moduli (μ) for the anterior and posterior walls of the arterial phantoms in the accuracy study for different freeze/thaw cycles and intraluminal pressures measured with shear wave elastography by phase velocity analysis above 500 Hz and with mechanical testing

		μ (kPa)		
Intraluminal pressure	Testing method	3 F/T cycles	4 F/T cycles	5 F/T cycles
60 mm Hg	SWE, anterior wall	40.4 ± 2.4	58.5 ± 1.2	55.9 ± 6.3
	SWE, posterior wall	41.6 ± 2.7	62.8 ± 2.7	60.1 ± 7.7
	MT	43.7 ± 4.5	58.3 ± 7.0	63.0 ± 2.6
80 mm Hg	SWE, anterior wall	49.8 ± 4.4	60.6 ± 6.2	66.8 ± 4.0
	SWE, posterior wall	50.3 ± 2.3	70.0 ± 9.3	68.3 ± 4.2
	MT	52.0 ± 3.6	66.7 ± 8.5	72.7 ± 7.1
100 mm Hg	SWE, anterior wall	53.3 ± 4.7	71.0 ± 6.3	75.3 ± 5.2
	SWE, posterior wall	56.3 ± 0.6	74.9 ± 8.5	74.1 ± 4.0
	MT	62.0 ± 2.6	75.7 ± 7.0	78.7 ± 5.5
120 mm Hg	SWE, anterior wall	62.6 ± 10	81.9 ± 5.4	81.0 ± 2.5
	SWE, posterior wall	64.3 ± 7.9	80.1 ± 15	94.0 ± 13
	MT	67.0 ± 5.7	75.0 ± 10	87.0 ± 2.6

F/T = freeze/thaw; MT = mechanical testing; SWE = shear wave elastography.

Table 4. Relative error between shear wave elastography and mechanical testing estimation of the phantom shear modulus*

	Relative error
Pressure	
60 mm Hg	9.9 ± 3.5
80 mm Hg	7.7 ± 2.4
100 mm Hg	8.4 ± 4.3
120 mm Hg	8.9 ± 2.5
Freeze/thaw cycles	
3	10.1 ± 3.9
4	8.2 ± 2.4
5	8.0 ± 2.8
Region of interest location	
Anterior	9.8 ± 3.6
Posterior	7.9 ± 2.7

* Measurements are grouped for different values of intraluminal pressure, number of freeze/thaw cycles and placement of the region of interest during shear wave elastography measurements.

phenomena were still induced in the phantom wall because the wavelengths of the generated shear waves were in the range of millimeters and, therefore, comparable to the phantom thickness. The motivation for constructing phantoms with walls thicker than those of human arteries is based on the manufacturing process and the experimental setup: thinner PVA phantoms would break and not withstand pressurization.

In addition to the confined geometry, tissue viscoelasticity is another cause of frequency dispersion in SWE applications in soft tissues (Amador et al. 2011; García et al. 2012). PVA has exhibited viscoelastic behavior when measured by atomic force microscopy (Yang 2008). However, this seems to be of minor importance because a previous simulation study using a plate model reported that moderate viscosity increased attenuation, but did not affect the dispersion curve (Nguyen et al. 2011). On the basis of these considerations, only dispersion phenomena caused by the geometry of the medium were considered in the accuracy study.

Even though the plate model does not fully characterize the cylindrical geometry of the arterial phantoms at low frequencies, the exact geometry becomes less relevant at higher frequencies as the wavelength of the Lamb wave becomes smaller compared with the hollow cylinder thickness (Couade et al. 2010). The characteristic local decrease in the dispersion curve depends on the thickness and diameter of the hollow cylinder and, therefore, always occurs in the same range of frequencies, for a given geometry. It has previously been suggested that a cutoff value of 1 kHz be used for arterial applications (Couade et al. 2010), but the intensity of the signal above this limit was too low to obtain reliable shear modulus estimations in the present study. The frequency bandwidth depends on the excitation duration and spatial beam width used to generate the shear wave (Palmeri et al. 2014), parameters that could not be controlled in the commercial system. As a result of these considerations, the choice of the lower cutoff frequency (500 Hz) was based on two criteria: preserve as much as possible of the signal's bandwidth and discard the characteristic local decrease in the hollow cylinder dispersion curve occurring between 400 and 500 Hz (Fig. 7a).

Although the SWE accuracy assessment was performed on phantoms, measured shear wave values are in agreement with those obtained by Bernal et al. (2011) in porcine carotid artery (range: 24–45 kPa) and by Couade et al. (2010) in a healthy individual during diastole (80 ± 10 kPa). However, arterial stiffness varies in a wide range of elastic shear modulus values, from a few kilopascals to hundreds of kilopascals (Deng et al. 1994; Kamenskiy et al. 2014). Complementary investigations with harder phantom material or *ex vivo* arteries should be carried out to fully assess SWE performance in arterial applications.

Mechanical testing

The general mechanical behavior of the PVA phantoms was evaluated in pre-studies. The material exhibited overall non-linear behavior, with quasi-linear behavior for small strain ranges (<10%). Hyperelastic constitutive models (neo-Hookean and Mooney–Rivlin) were also tested, with results similar to those of linear theory in the strain ranges evaluated. Therefore, the material can be considered to behave linearly close to the general mechanical stress state created by the intraluminal pressure and the imposed longitudinal strain.

Concerning the mechanical testing for the geometry study, tests on a large sample solid cylinder were used as a reference for the three geometries because the phantom material was the same among the large sample cylinder and the other geometries (PVA solution from the same batch) and the phantoms had the same stress configuration (*i.e.*, neither pressurization nor load was applied). The shear modulus is an intrinsic material parameter and does not depend on the geometry of the sample.

Concerning the mechanical testing for the accuracy study, experimental standards provided by the American Society for Testing and Materials suggest the use of angular twist of a tubular sample when assessing elastic shear properties (ASTM 2008). Despite this, as stated in the standard, the test method is designated for structural materials and may not suffice in describing similar behavior of soft tissue or rubber samples. If assessing tubular samples of soft tissue or tissue-mimicking phantoms, twisting may induce torsional buckling (representing a non-linear change in mechanical energy), which further complicates the assessment of elastic properties

(Ertepinar and Wang 1975). In the light of these considerations, mechanical testing based on tensile strain was chosen as a reference method in this study. The material's tensile mechanical properties were then used to derive shear properties, following valid assumptions of incompressibility and homogeneity of PVA previously shown (Fromageau et al. 2003). The agreement between mechanical testing and SWE measurements indicates that no assumption of the mechanical behavior was significantly violated.

Limitations

Several limitations should be addressed before generalizing results from this controlled *in vitro* study to clinical applications *in vivo*. In contrast to the arterial phantoms, vascular tissue is strongly anisotropic with complex fiber orientation, which will influence wave propagation in the artery (Urban et al. 2013). Additionally, the pressure in arteries is not static, but dynamically varying due to the pulse wave of the blood traveling through the arterial system during the cardiac cycle. However, because the scales of the pulse wave (1 s) and the shear wave (10^{-3} s) differ in magnitude, it is possible to remove the pulse wave motion before performing SWE measurement, as previously reported (Couade et al. 2010). The next step in the validation of SWE for arterial applications should therefore include dynamic tests and take anisotropy into account. An *ex vivo* study would enable investigation of anisotropic material and more realistic stiffness values. Additionally, the effect of the surrounding tissue on push intensity and signal bandwidth should be addressed before *in vivo* measurements can be performed with confidence. Finally, an algorithm with the ability to track the shear waves when the artery is not aligned parallel to the transducer surface would make the technique more flexible and robust for future clinical applications.

CONCLUSIONS

This study indicated that SWE and phase velocity analysis can accurately measure stiffness in arterial phantoms when validated against mechanical testing. SWE measurements based on phase velocity analysis were in good agreement with those of mechanical testing and had an average relative error of 8.8 ± 6.0%, independent of applied intraluminal pressure, phantom stiffness or ROI location. To the contrary, group velocity with an infinite medium assumption incorrectly estimated shear modulus values in confined geometries and should therefore not be used in arterial applications.

Acknowledgments—This study was supported by VINNOVA VINNMER Marie Curie International Qualification Grant 2011-01365 and Swedish Research Council Grant 2012-2795. The authors thank Peter Arfert for his precious help with the experimental setup.

REFERENCES

Amador C, Urban MW, Chen S, Chen Q, An KN, Greenleaf JF. Shear elastic modulus estimation from indentation and SDUV on gelatin phantoms. IEEE Trans Biomed Eng 2011;58:1706–1714.

American Society for Testing and Materials (ASTM). ASTM E143-02 Standard test method for shear modulus at room temperature [WWW Document]. Available at: http://enterprise.astm.org/filtrexx40.cgi?HISTORICAL/E143-02R08.htm; 2008. Accessed July 14, 2014.

Bercoff J, Tanter M, Fink M. Supersonic shear imaging: a new technique for soft tissue elasticity mapping. IEEE Trans Ultrason Ferroelectr Freq Control 2004a;51:396–409.

Bercoff J, Tanter M, Fink M. Sonic boom in soft materials: The elastic Cerenkov effect. Appl Phys Lett 2004b;84:2202.

Bernal M, Nenadic I, Urban MW, Greenleaf JF. Material property estimation for tubes and arteries using ultrasound radiation force and analysis of propagating modes. J Acoust Soc Am 2011;129:1344–1354.

Brands PJ, Willigers JM, Ledoux LAF, Reneman RS, Hoeks APG. A noninvasive method to estimate pulse wave velocity in arteries locally by means of ultrasound. Ultrasound Med Biol 1998;24:1325–1335.

Chang JM, Moon WK, Cho N, Yi A, Koo HR, Han W, Noh DY, Moon HG, Kim SJ. Clinical application of shear wave elastography (SWE) in the diagnosis of benign and malignant breast diseases. Breast Cancer Res Treat 2011;129:89–97.

Chen S, Fatemi M, Greenleaf JF. Quantifying elasticity and viscosity from measurement of shear wave speed dispersion. J Acoust Soc Am 2004;115:2781.

Couade M, Pernot M, Prada C, Messas E, Emmerich J, Bruneval P, Criton A, Fink M, Tanter M. Quantitative assessment of arterial wall biomechanical properties using shear wave imaging. Ultrasound Med Biol 2010;36:1662–1676.

Coutinho T. Arterial stiffness and its clinical implications in women. Can J Cardiol 2014;30:756–764.

Deng SX, Tomioka J, Debes JC, Fung YC. New experiments on shear modulus of elasticity of arteries. Am J Physiol 1994;266(1, Pt 2):H1–H10.

Ertepinar A, Wang ASD. Torsional buckling of an elastic thick-walled tube made of rubber-like material. Int J Solids Struct 1975;11:329–337.

Ferraioli G, Parekh P, Levitov AB, Filice C. Shear wave elastography for evaluation of liver fibrosis. J Ultrasound Med 2014;33:197–203.

Fromageau J, Brusseau E, Vray D, Gimenez G, Delachartre P. Characterization of PVA cryogel for intravascular ultrasound elasticity imaging. IEEE Trans Ultrason Ferroelectr Freq Control 2003;50:1318–1324.

Fromageau J, Gennisson JL, Schmitt C, Maurice RL, Mongrain R, Cloutier G. Estimation of polyvinyl alcohol cryogel mechanical properties with four ultrasound elastography methods and comparison with gold standard testings. IEEE Trans Ultrason Ferroelectr Freq Control 2007;54:498–509.

García A, Martínez MA, Peña E. Viscoelastic properties of the passive mechanical behavior of the porcine carotid artery: Influence of proximal and distal positions. Biorheology 2012;49:271–288.

Garrard JW, Ramnarine K. Shear-wave elastography in carotid plaques: Comparison with grayscale median and histological assessment in an interesting case. Ultraschall Med 2014;35:1–3.

Gazis DC. Three-dimensional investigation of the propagation of waves in hollow circular cylinders: I. Analytical foundation. J Acoust Soc Am 1959a;31:568.

Gazis DC. Three-dimensional investigation of the propagation of waves in hollow circular cylinders: II. Numerical results. J Acoust Soc Am 1959b;31:573.

Glasser S. Vascular compliance and cardiovascular disease: A risk factor or a marker? Am J Hypertens 1997;10:1175–1189.

Hamilton PK, Lockhart CJ, Quinn CE, McVeigh GE. Arterial stiffness: Clinical relevance, measurement and treatment. Clin Sci (Lond) 2007;113:157–170.

Hoeks AP, Brands PJ, Smeets FA, Reneman RS. Assessment of the distensibility of superficial arteries. Ultrasound Med Biol 1990;16:121–128.

Kamenskiy AV, Dzenis YA, Kazmi SAJ, Pemberton MA, Pipinos II, Phillips NY, Herber K, Woodford T, Bowen RE, Lomneth CS, MacTaggart JN. Biaxial mechanical properties of the human thoracic and abdominal aorta, common carotid, subclavian, renal and common iliac arteries. Biomech Model Mechanobiol 2014;13: 1341–1359.

Kawasaki T, Sasayama S, Yagi S, Asakawa T, Hirai T. Non-invasive assessment of the age related changes in stiffness of major branches of the human arteries. Cardiovasc Res 1987;21:678–687.

Khamdaeng T, Luo J, Vappou J, Terdtoon P, Konofagou EE. Arterial stiffness identification of the human carotid artery using the stress–strain relationship in vivo. Ultrasonics 2012;52:402–411.

Kim DH, Braam B. Assessment of arterial stiffness using applanation tonometry. Can J Physiol Pharmacol 2013;91:999–1008.

Larsson M, Heyde B, Kremer F, Brodin LÅ, D'hooge J. Ultrasound speckle tracking for radial, longitudinal and circumferential strain estimation of the carotid artery: An in vitro validation via sonomicrometry using clinical and high-frequency ultrasound. Ultrasonics 2015;56:399–408.

Loupas T, Powers JT, Gill RW. An axial velocity estimator for ultrasound blood flow imaging, based on a full evaluation of the Doppler equation by means of a two-dimensional autocorrelation approach. IEEE Trans Ultrason Ferroelectr Freq Control 1995;42:672–688.

Nenadic IZ, Qiang B, Urban MW, de Araujo Vasconcelo LH, Nabavizadeh A, Alizad A, Greenleaf JF, Fatemi M. Ultrasound bladder vibrometry method for measuring viscoelasticity of the bladder wall. Phys Med Biol 2013;58:2675–2695.

Nguyen TM, Couade M, Bercoff J, Tanter M. Assessment of viscous and elastic properties of sub-wavelength layered soft tissues using shear wave spectroscopy: theoretical framework and in vitro experimental validation. IEEE Trans Ultrason Ferroelectr Freq Control 2011;58: 2305–2315.

Palmeri ML, Rouze NC, Nightingale KR. Dependence of shear wave spectral content on acoustic radiation force excitation duration and spatial beamwidth. Proc IEEE Int Ultrason Symp 2014;1105–1108.

Pinton GF, Dahl JJ, Trahey GE. Rapid tracking of small displacements with ultrasound. IEEE Trans Ultrason Ferroelectr Freq Control 2006;53:1103–1117.

Quinn U, Tomlinson LA, Cockcroft JR. Arterial stiffness. JRSM Cardiovasc Dis 2012;1:1–8.

Ramnarine KV, Garrard JW, Dexter K, Nduwayo S, Panerai RB, Robinson TG. Shear wave elastography assessment of carotid plaque stiffness: In vitro reproducibility study. Ultrasound Med Biol 2014;40:200–209.

Ribbers H, Lopata RGP, Holewijn S, Pasterkamp G, Blankensteijn JD, de Korte CL. Noninvasive two-dimensional strain imaging of arteries: Validation in phantoms and preliminary experience in carotid arteries in vivo. Ultrasound Med Biol 2007;33:530–540.

Sarvazyan AP, Urban MW, Greenleaf JF. Acoustic waves in medical imaging and diagnostics. Ultrasound Med Biol 2013;39:1133–1146.

Shcherbakova DA, Papadacci C, Swillens A, Caenen A, De Bock S, Saey V, Chiers K, Tanter M, Greenwald SE, Pernot M, Segers P. Supersonic shear wave imaging to assess arterial nonlinear behavior and anisotropy: Proof of principle via ex vivo testing of the horse aorta. Adv Mech Eng 2014;6:1–12.

Song P, Zhao H, Urban M, Manduca A, Pislaru S, Kinnick R, Pislaru C, Greenleaf J, Chen S. Improved shear wave motion detection using pulse-inversion harmonic imaging with a phased array transducer. IEEE Trans Med Imaging 2013;32:2299–2310.

Tanter M, Touboul D, Gennisson JL, Bercoff J, Fink M. High-resolution quantitative imaging of cornea elasticity using supersonic shear imaging. IEEE Trans Med Imaging 2009;2:1881–1893.

Urban MW, Nenadic IZ, Pislaru C, Greenleaf JF. Measurement of longitudinal and circumferential waves in tubes and artery excited with ultrasound radiation force. Proc 2013 IEEE Int Ultrason Symp 2013;1765–1768.

Vlachopoulos C, Aznaouridis K, Stefanadis C. Prediction of cardiovascular events and all-cause mortality with arterial stiffness: A systematic review and meta-analysis. J Am Coll Cardiol 2010;55: 1318–1327.

Woodrum DA, Romano AJ, Lerman A, Pandya UH, Brosh D, Rossman PJ, Lerman LO, Ehman RL. Vascular wall elasticity measurement by magnetic resonance imaging. Magn Reson Med 2006; 56:593–600.

Xu L, Chen J, Yin M, Glaser KJ, Chen Q, Woodrum DA, Ehman RL. Assessment of stiffness changes in the ex vivo porcine aortic wall using magnetic resonance elastography. Magn Reson Imaging 2012; 30:122–127.

Yang N. Viscoelastic properties of poly(vinyl alcohol) nanofibres and hydrogels measured by atomic force microscopy. Phys Canada 2008;64:141–143.